High-order-harmonic spectra from atoms in intense laser fields: Exact versus approximate methods

S. N. Pugliese,[1] A. S. Simonsen,[2] M. Førre,[2] and J. P. Hansen[1,2]
[1]*CONICET and Centro Atómico Bariloche, Comisión Nacional de Energía Atómica, Avenida Exequiel Bustillo 9500, 8400 Bariloche, Argentina*
[2]*Department of Physics and Technology, University of Bergen, N-5007 Bergen, Norway*
(Received 9 February 2015; published 31 August 2015)

We compare harmonic spectra from hydrogen based on the numerical solution of the time-dependent Schrödinger equation and three approximate models: (i) the strong field approximation (SFA), (ii) the Coulomb-Volkov modified strong field approximation (CVA), and (iii) the strong field approximation with the stationary phase approximation applied to the momentum integrals (SPSFA). At laser intensities in the range of $(1-3)\times 10^{14}$ W/cm^2 we find good agreement when comparing the SFA and CVA with exact results. In general the CVA displays an overall better agreement with *ab initio* results, which reflects the role of the Coulomb field in the ionization as well as in the recombination process. Furthermore, it is found that the widely used SPSFA breaks down for low-order harmonic generation; i.e., the approximation turns out to be accurate only in the outer part of the harmonic plateau region as well as in the cutoff region. We trace this deficiency to the singularity of the SPSFA associated with short trajectories, i.e., short return times. When removing these, we obtain a version of the SPSFA which works rather well for the entire harmonic spectrum.

DOI: 10.1103/PhysRevA.92.023424 PACS number(s): 32.80.Wr, 42.65.Ky, 42.50.Hz

I. INTRODUCTION

High harmonic generation (HHG) of photons during interaction between atoms and intense laser fields has its phenomenological origin [1] and quantum mechanical explanation [2] from about 20 years ago. At that time the basic cutoff law, i.e., the relation between the highest photon frequencies generated and the laser intensity and driving frequency, was established both classically and based on the stationary phase method applied to the strong field approximation. Since then, HHG in molecules [3–6], extended systems [7,8], and solids [9] has opened new aspects with regard to both the cutoff laws and the production of attosecond light [10] with tunable polarization. Nevertheless, the basic mechanism of HHG from simple atoms with linear polarized light sources is still debated, in particular, the role of the binding potential [11].

When it comes to the quantum mechanical description it is obvious that harmonic spectra based on accurate solutions of the time-dependent Schrödinger equation (TDSE) are limited to one active electron systems and in a few cases to two active electron systems. In addition to the numerical challenges associated with solving the TDSE directly, the application of *ab initio* methods is limited to systems where an accurate description of the potential is available. Approximate models on the other hand, like, e.g., the widely used strong field approximation (SFA), can relatively straightforwardly be applied to complex molecular systems without detailed knowledge of the potential, as it only requires a sufficiently accurate representation of the initial state. Nevertheless, the detailed comparison between HHG spectra from such approximate methods and exact results are relatively few [12,13]. Also, it is well established [14–18] that Coulomb corrections in the continuum state, leading to the so-called Coulomb-Volkov approximation (CVA), allow for some accounting of the remaining core and thus describe ionization more accurately. In the SFA, on the other hand, the influence of the core is neglected, i.e., the continuum states are eigenstates of a free electron in the time-dependent electric field. Introducing an additional approximation on the resulting SFA integrals, i.e., the so-called stationary phase approximation, the stationary phase strong field approximation (SPSFA) is obtained. A related comparison of the CVA, the SFA, and the TDSE for differential electron emission in laser fields was performed some time ago [19], and this study showed that the CVA performed much better than the SFA. At present, there exist a variety of models based on Coulomb-Volkov type states for atomic ionization by ultrashort laser pulses, e.g., the modified Coulomb-Volkov approach that uses an initial bound state which takes into account transitions to intermediate bound states, allowing the multiphoton ionization process to occur from these levels [20]. The double-distorted Coulomb-Volkov approximation is another example, which includes the distortion by the laser field in the initial state, accounting for dynamic Stark effects in the presence of the field [21].

Coulomb corrections were introduced in the SFA model for the calculation of high-harmonic spectra in several works [22–24], but it is still an open question whether the CVA approach is more suitable for HHG as compared to the SFA. Another aspect regarding HHG is the reliability of the commonly used stationary phase approximation (SPA) to the electron momentum integral [23–25]. The theory here contains an adjustable parameter which has to be introduced to keep integrals finite. To the extent that the harmonic spectrum depends on this parameter, attempts to describe structures in the harmonic spectrum should be performed with care [26].

In this work, we perform a detailed comparison between the CVA and the SFA, the latter calculated with and without the SPA. HHG spectra at three characteristic peak laser intensities $[(1-3)\times 10^{14}$ W/cm$^2]$ are compared with exact spectra from the TDSE. It will be shown that the CVA is in general in best agreement with the *ab initio* result. However, also the SFA is reasonable in describing the general shape of the harmonic spectrum, in particular, in the cutoff region.

The standard SPSFA approach, on the other hand, turns out to be valid only around the cutoff and needs to be modified in order to capture the exact SFA result in the lower part

of the harmonic spectrum. The origin of the fault lies in the use of the saddle point approximation when calculating the momentum integrals within the SFA. This leads to an inherent divergence in the resulting harmonic signal which is usually circumvented by introducing a regularization parameter [2]. We show that the final result is sensitive to the actual choice of regularization, in particular, in the lower-harmonic region. It is generally assumed that the SFA fails, due to the missing influence of the Coulomb potential in the model, in situations where the electron only spends a short time in the continuum before it recombines, i.e., for very short trajectories leading to the emission of lower-order harmonics. We demonstrate that the standard SPSFA can be significantly improved simply by removing all trajectories from the model corresponding to the electron spending only some fraction of a field cycle in the continuum. In the next section we describe the numerical models and in the following one we discuss the detailed results. Atomic units ($e = \hbar = m_e = a_0 = 1$) are used unless explicitly otherwise mentioned.

II. NUMERICAL MODELS

The starting point is the time-dependent Hamiltonian describing a hydrogen atom interacting with a driving electromagnetic pulse described by the vector potential $\mathbf{A}(t)$. In the velocity gauge form and within the dipole approximation the TDSE reads as follows:

$$\left[\frac{1}{2}[\mathbf{p} + \mathbf{A}(t)]^2 - \frac{1}{r} - i\partial_t\right]\Psi(\mathbf{r},t) = 0. \tag{1}$$

Performing a phase transformation of the wave function, $\Psi \longrightarrow \exp[-i\int_0^t A^2(t')dt']\Psi$, an effective Hamiltonian, $H(t) = H_0 + \mathbf{A}(t)\cdot\mathbf{p}$, is obtained, where H_0 represents the field-free atomic part. The case of 800-nm laser light ($\omega_0 = 0.057$ a.u.) is treated in the present work with a linear polarization of the electric field along the z axis, $\mathbf{A}(t) = A(t)\hat{\mathbf{z}}$. We consider a flat-top pulse with a sine-squared ramp-on and ramp-off at the temporal edges:

$$A(t) = \begin{cases} A_0 \sin^2\left(\frac{t\pi}{2T_r}\right)\sin(\omega_0 t), & 0 \leqslant t \leqslant T_r, \\ A_0 \sin(\omega_0 t), & T_r < t < T - T_r, \\ A_0 \sin^2\left(\frac{(T-t)\pi}{2T_r}\right)\sin(\omega_0 t), & T - T_r \leqslant t \leqslant T, \\ 0, & \text{elsewise}, \end{cases} \tag{2}$$

where $T_r = 5.31$ fs is the ramp duration and $T = 21.25$ fs is the full pulse duration leaving an intermediate flat-top region of 10.63 fs. In terms of optical cycles, the ramp and intermediate pulse durations correspond to two and four cycles, respectively. The amplitude A_0 is the value of the vector potential when the laser is at peak brilliance. The TDSE [Eq. (1)] interacting with the field described in Eq. (2) is solved in a basis of radial B-spline functions and spherical harmonics,

$$\Psi(\mathbf{r},t) = \sum_{k,l} c_{k,l}(t)\frac{B_k(r)}{r}Y_l^{m=0}(\Omega), \tag{3}$$

where $B_k(r)$ is the kth B-spline function and $Y_l^{m=0}(\Omega)$ is the standard spherical harmonic for the solid angle. From the initial ground-state vector $\mathbf{c}(t=0)$, obtained by diagonalization of the Hamiltonian matrix, the vector of coefficients $\mathbf{c}(t)$ is propagated in time throughout the laser-atom interaction with the following scheme:

$$\mathbf{c}(t+\Delta t) = \left(\mathbf{S} + \frac{i\Delta t}{2}\mathbf{H}(t+\Delta t)\right)^{-1}\left(\mathbf{S} - \frac{i\Delta t}{2}\mathbf{H}(t)\right)\mathbf{c}(t), \tag{4}$$

where Δt is the propagator time-step and $\mathbf{S}$ and $\mathbf{H}$ are the matrices associated with the basis overlap and the Hamiltonian operator, respectively. Equation (4) in its present form is manifestly nonunitary, with the consequence that the norm of the wave function is not conserved *per se*, as opposed to the unitary time-synchronized version of the propagator [27]. However, the nonunitary scheme provides a practical means for controlling the truncation error committed in the time integration in that the stability of the wave function norm is monitored during the propagation. More details regarding our computational scheme for solving the TDSE can be found in Ref. [28].

The HHG spectra $I_{\text{rad}}(\omega)$ are here obtained by taking the Fourier transform of the time-sampled expectation value of the momentum operator [29],

$$I_{\text{rad}}(\omega) = \left|\hat{\mathbf{n}}\cdot\int_{-\infty}^{\infty} W(t)\langle\Psi(\mathbf{r},t)|\,\mathbf{p}\,|\Psi(\mathbf{r},t)\rangle e^{-i\omega t}\,dt\right|^2, \tag{5}$$

where $\hat{\mathbf{n}}$ is the unit direction and $W(t)$ is a finite window function. Strictly speaking, the expectation value of the momentum should be calculated as $\langle\Psi(\mathbf{r},t)|\,\mathbf{p}+\mathbf{A}\,|\Psi(\mathbf{r},t)\rangle$. However, the contribution from the second term, i.e., the $\mathbf{A}$ term, is unimportant for all harmonics but the first (at the fundamental frequency). Provided the wave function is exact, the expectation value (5) is gauge independent, and there exists a one-to-one correspondence between the spectrum obtained using the dipole, the dipole velocity, or the dipole acceleration form of the expectation value [29]. Within the SFA this is not necessarily the case; i.e., the length and velocity gauge forms may differ and care should be taken when calculating the spectrum. Nevertheless, in the present study of HHG in hydrogen we have found that the dipole and dipole velocity forms of the expectation value result in similar spectra, and therefore the velocity form Eq. (5) has been applied throughout. The time-dependent wave function is obtained within the velocity gauge, i.e., Eq. (1). This choice of gauge is well known to be numerically most efficient in terms of basis size in the exact treatment. Furthermore, within the SFA, it does not contain spurious coupling terms for extended systems, as, for example, is the case within the length gauge formulation [8,30,31].

The following cosine expansion is used as a window function in Eq. (5),

$$W(t) = \sum_{n=0}^{n\leqslant 4}(-1)^n a_n \cos\left(2n\frac{\pi t}{T}\right), \tag{6}$$

where the coefficients are set to $a_0 = 0.209\,671$, $a_1 = 0.407\,331$, $a_2 = 0.281\,225$, $a_3 = 0.092\,669$, and $a_4 = 0.009\,104$. This particular form is called the minimum side lobe five-term flat-top window (MS-5FT) in Ref. [32]. Although a different choice of window function, e.g., the commonly used Gaussian window, would suffice, the MS-5FT window is chosen here for two reasons. First, the MS-5FT window

results in relatively narrow harmonic peaks, and second, the peaks are separated by "deep valleys," making the individual radiation yield at each harmonic order clearly distinguishable from the neighboring harmonics. This is advantageous when comparing harmonic spectra obtained with different models.

The model approaches are based on expanding the wave function in a superposition of the (unperturbed) ground state and a complete set of (field-dressed) continuum states, i.e.,

$$\Psi(\mathbf{r},t) = c_{1s}(t)\Psi_{1s}(\mathbf{r},t) + \int c_k(t)\Psi_k^f(\mathbf{r},t)d^3k, \qquad (7)$$

where $\Psi_{1s}(\mathbf{r},t) = \psi_{1s}(\mathbf{r})\,e^{-iE_it}$, with $E_i = -0.5$ a.u. The models are derived by assuming negligible depletion of the initial state, i.e., $c_{1s}(t) \simeq 1$, as well as neglecting the overlap in the basis due to the over completeness, and then writing the amplitude of the continuum wave in the approximate first-order form,

$$c_k(t) = -i\int_{-\infty}^{t} \langle \Psi_k^f(\mathbf{r},t')|\ \mathbf{A}(t')\cdot\mathbf{p}|\Psi_{1s}(\mathbf{r},t')\rangle dt'. \qquad (8)$$

The two models, SFA and CVA, are obtained with two different sets of continuum basis functions Ψ_k^f. We start with the Volkov wave function, describing an electron at time t' moving in the electromagnetic field only,

$$\Psi_k^{f=V}(\mathbf{r},t') = \frac{1}{(2\pi)^{3/2}}e^{i[\mathbf{k}\cdot\mathbf{r}-S(\mathbf{k},t',t_0)]} = \psi_k^V(\mathbf{r})e^{-iS(\mathbf{k},t',t_0)}, \qquad (9)$$

where t_0 is a common (arbitrary) reference time for the Volkov states, and the action $S(\mathbf{k},t',t_0) = \frac{1}{2}\int_{t_0}^{t'}[\mathbf{k}+\mathbf{A}(t'')]^2dt''$. By augmenting these functions with Coulomb phases it is argued that effects of the Coulomb potential are taken into account [14]. The description of the electron propagating in the continuum then becomes

$$\Psi_k^{f=\mathrm{CV}}(\mathbf{r},t') = \psi_k^{\mathrm{CV}}(\mathbf{r})e^{-iS(\mathbf{k},t',t_0)} = e^{1/2\pi\beta}\Gamma(1+i\beta)\,{}_1F_1(-i\beta,1,-1kr-ikr) \times \psi_k^V(\mathbf{r})e^{-iS(\mathbf{k},t',t_0)}, \qquad (10)$$

where $\beta = Z/k$ is the Sommerfeld parameter, Γ is the gamma function, and ${}_1F_1$ is the confluent hypergeometric function. Inserting Eq. (8) into the expansion (7) and using that $\Psi_k^f(\mathbf{r},t') = \psi_k^f(\mathbf{r})e^{-iS(\mathbf{k},t',t_0)}$, we arrive at the following expression for the momentum expectation value:

$$\langle\Psi|\,\mathbf{p}\,|\Psi\rangle = 2\mathrm{Re}\left\{-i\int_{-\infty}^{t} e^{iE_i(t-t')} \times\left[\int R_{\mathrm{ion}}(\mathbf{k},t')V_{\mathrm{rec}}(\mathbf{k})\,e^{-iS(\mathbf{k},t,t')}d^3k\right]dt'\right\}. \qquad (11)$$

Here, the contributions from the (small) continuum-continuum term have been neglected and the ionization amplitude at time t' and the corresponding recombination amplitude at time t are, respectively, given by

$$R_{\mathrm{ion}}(\mathbf{k},t') = \mathbf{A}(t')\int \psi_k^{f*}(\mathbf{r})\ \mathbf{p}\ \psi_{1s}(\mathbf{r})d^3r, \qquad (12)$$

$$V_{\mathrm{rec}}(\mathbf{k}) = \int \psi_{1s}^*(\mathbf{r})\ \mathbf{p}\ \psi_k^f(\mathbf{r})d^3r. \qquad (13)$$

Using $\Psi^{f=V}$ as basis functions in Eq. (7) results in the SFA while the use of the $\Psi^{f=\mathrm{CV}}$ continuum functions defines the CVA. These basis functions lead to different ionization (R_{ion}) and recombination (V_{rec}) amplitudes. In both cases they result in analytical expressions:

$$R_{\mathrm{ion}}^V(\mathbf{k},t') = \mathbf{A}(t')\frac{2\sqrt{2}k\cos(\theta_k)}{\pi(1+k^2)^2}. \qquad (14)$$

With Coulomb phases the result is slightly more complex [33],

$$R_{\mathrm{ion}}^{\mathrm{CV}}(\mathbf{k},t') = \mathbf{A}(t')\frac{2\sqrt{2}}{\pi}\frac{k}{(1+k^2)^2}\cos(\theta_k)e^{(1/2\pi\beta)} \times\Gamma(1-i\beta)\left(1-\frac{2k(i+k)}{1+k^2}\right)^{-i\beta}(1-i\beta). \qquad (15)$$

We note that Eq. (15) reduces to the SFA result in the limit of $\beta \to 0$ as expected. For finite β the Volkov and the Coulomb-Volkov wave functions are independently normalized, which is a prerequisite in order to perform a one-to-one comparison between the two resulting HHG spectra.

To minimize the computational effort the stationary phase approximation is usually invoked in order to solve the momentum integrals. It involves accounting for only the momentum of electrons which are born at some position at time t' and return to the same position at a later time t. This gives a final time integral left which involves the stationary phase momentum $\mathbf{k}_s = -\int_{t'}^{t}\mathbf{A}(t'')dt''/(t-t')$. The momentum expectation value is then found as

$$\langle\Psi|\mathbf{p}|\Psi\rangle = 2\mathrm{Re}\left\{-i\int_{-\infty}^{t} e^{iE_i(t-t')}R_{\mathrm{ion}}(\mathbf{k_s},t')V_{\mathrm{rec}}(\mathbf{k_s}) \times e^{-iS(\mathbf{k_s},t,t')}\left(\frac{2\pi}{i(t-t')+\epsilon}\right)^{3/2}dt'\right\}. \qquad (16)$$

The regularization parameter ϵ is here an ad hoc quantity introduced to keep the integrals finite at $t = t'$, and the precise value of it has generally been believed to be unimportant for the HHG spectrum [2]. However, our calculations show that this is only true for the harmonic spectrum around the cutoff region. In the limit of vanishingly small ϵ the integral in Eq. (16) diverges due to the singularity in the denominator. The divergence appears in the limit $t \to t'$ and originates from the contribution of electron trajectories where the electron spends an infinitesimal time in the continuum before it recombines, giving rise to lower-order harmonics.

The physics of the three HHG models is illustrated in Fig. 1. All the model approaches considered here conceptually share the same three-step mechanism from which they are derived: (a) ionization at time t', (b) acceleration in the field during the interval $t-t'$, and (c) recombination at time t. This three-step mechanism is shown in the top panel together with the time evolution of the eight-cycle 800-nm laser pulse. Also shown is the temporal shape of the applied window function (in blue). The three methods are shown in the next three panels of Fig. 1, in descending order based on the degree of approximation made in each scheme. The second panel shows the most sophisticated approximate model considered, namely, the CVA method. Here, the electron is during step (b) accelerated in a potential which comprises both the interaction with the laser and the Coulomb potential.

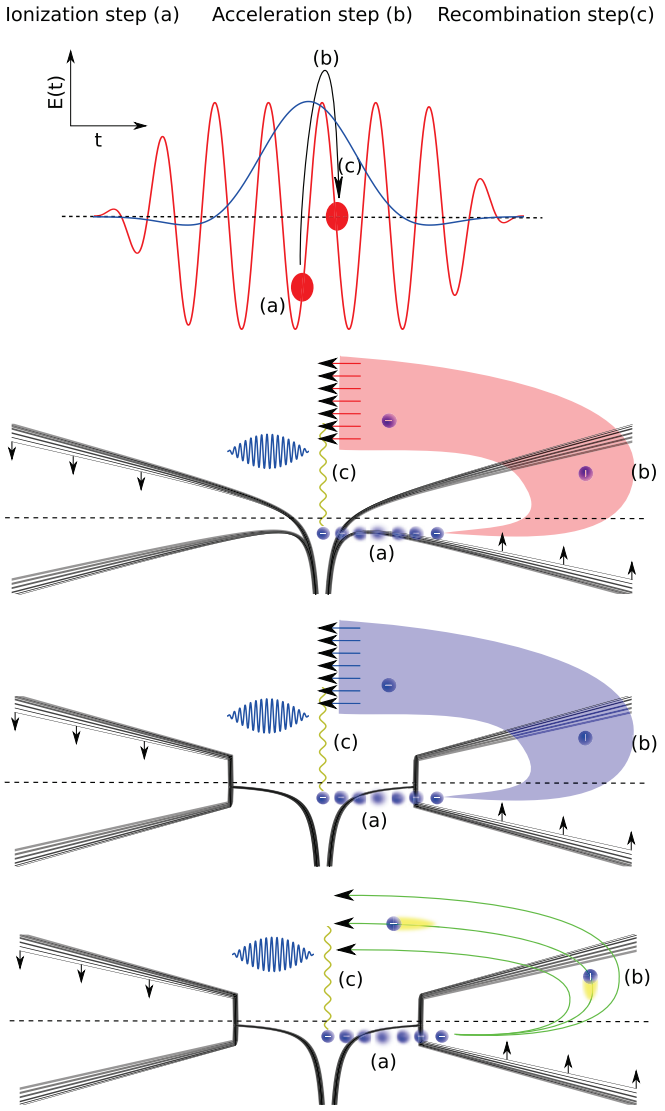

FIG. 1. (Color online) Schematic illustration of the three approximate models used to predict the HHG spectrum in the present work. In the top panel, the 800-nm laser pulse is drawn (red line) together with the time-dependent window function (blue line) used in the spectral analysis. The three approximations follow a three-step model: (a) ionization at time t', (b) acceleration in the laser field, and (c) recombination at time t with emission of high-harmonic light. The models are illustrated in descending order from most to least sophisticated in terms of the level of approximation and, as such, expected accuracy. Second panel from the top: The CVA method where the electron during step (b) propagates in the combined potential of the laser and the nucleus. Third panel from the top: Illustration of the SFA approach where the Coulomb potential generated by the nucleus is neglected when the electron resides in the continuum. Bottom panel: The SFA method with the stationary phase approximation applied to the momentum integrals. Here the recombination amplitude is restricted to contributions from (discrete) stationary phase momenta, depicted by individual (green) trajectory lines.

The total recombination amplitude is taken as the integral over a continuum of momenta, illustrated by the thick (red) layer in the figure. The next panel shows the SFA method where the Coulomb potential is only present in the initial ground state and neglected during the acceleration step (b). In this method, integration over the Volkov-continuum contributions is performed numerically which is illustrated by the (blue) shaded area of trajectories. Last, the lower panel depicts the presumably least accurate method, namely, the SFA method with the SPA applied to the momentum integrals. The electron is again assumed to propagate only in the potential due to the laser once ionized, but as opposed to the full SFA, only a restricted set of stationary phase momenta associated with recombination at a particular time t is included (depicted as discrete green trajectory lines).

In the next section we display results based on calculations performed within the SFA and CVA directly as well as for the SFA when the stationary phase argument is invoked. The results are compared with spectra obtained by solving the TDSE on an absolute scale which provide a reference calculation for both the shape and the strength of each harmonic.

III. RESULTS AND DISCUSSION

We now present the spectra of the high-order-harmonic radiation generated when atomic hydrogen is exposed to 800-nm laser light in the intensity regime $I_0 = (1-3) \times 10^{14}$ W/cm^2. The lower intensity is chosen high enough for generating a pronounced harmonic yield, but still low enough for differences in the spectra to appear when including or excluding Coulomb corrections. From here we increase the laser intensity to investigate to which extent these corrections become less important with stronger fields. Nevertheless, we restrict the highest intensity to 3×10^{14} W/cm^2 as saturation effects may become important, thus obstructing a direct comparison between the approximate results and the *ab initio* calculations to be made.

Concerning convergence issues of the different approaches, the TDSE produces fully converged results for all considered intensities using a basis including angular momenta up to $l_{\max} = 41$ and with a radial representation consisting of 6000 B splines distributed in a radial box of size $R = 3200$ a.u. The size of the radial box is chosen to be sufficiently large in order to completely contain the ionized wave packet during the laser-atom interaction, thus preventing unphysical reflections at the grid boundary responsible for artificial contributions to the momentum expectation value. In the SFA and CVA approaches, the numerical convergence is determined by the choice of discretization in the k^3 and t integrals [cf., Eq. (11)]. Here, we have included 2^{18} and 2^{12} discrete values of momentum and time, respectively, and increasing these numbers does not influence the results. The large number of integration points is necessary due to the highly oscillatory kernel functions. It implies that the approximate calculations (full SFA and CVA) become quite time-consuming. However, when the SPSFA is applied, the number of included electron trajectories or allowed momenta is directly determined by the discretized number of possible start and stop times [cf. Eq. (16)], i.e., the discretization in time, which of course reduces the numerical labor significantly. A few hundred thousand time steps (corresponding to the number of trajectories included) were made necessary in order to obtain fully converged SPSFA results for the smallest value of the

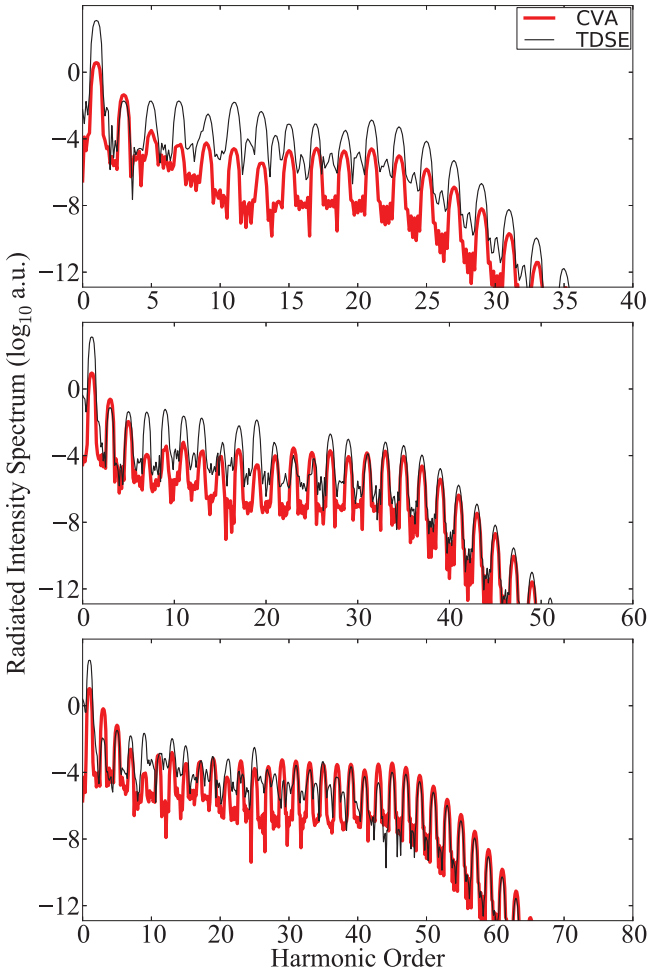

FIG. 2. (Color online) HHG spectrum as obtained by Eq. (5), given in atomic units and shown on a logarithmic scale. The CVA result (thick red line) is compared with the exact TDSE results (thin black line) at three different peak laser intensities: $I_0 = 1 \times 10^{14}$ W/cm^2 (top panel), $2I_0$ (middle panel), and $3I_0$ (lower panel).

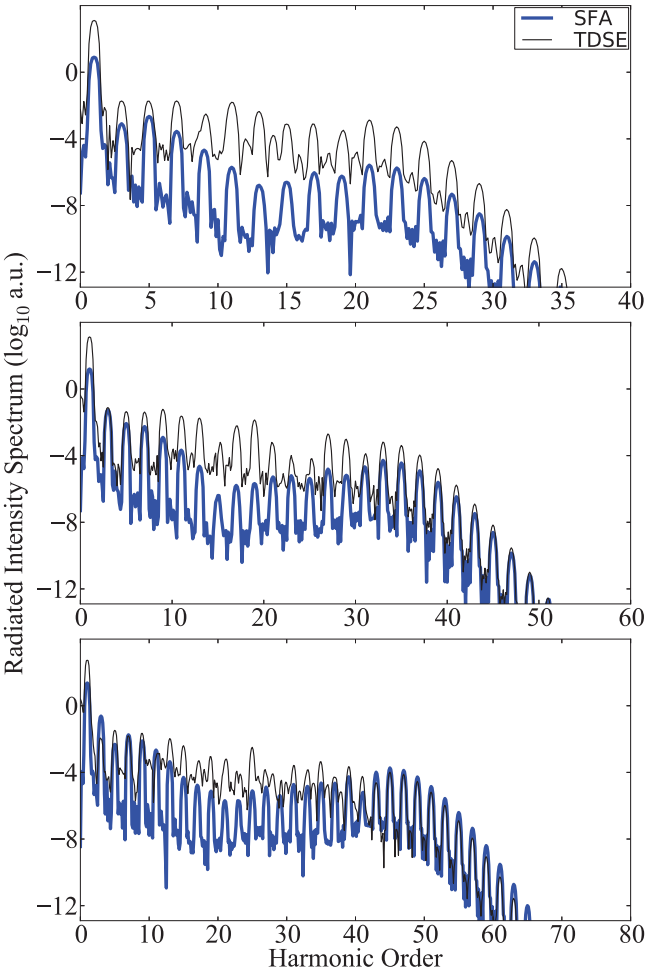

FIG. 3. (Color online) HHG spectrum, $I_{\rm rad}(\omega)$ [Eq. (5)], plotted on a logarithmic scale, from the SFA method (thick blue line) compared with the exact TDSE results (thin black line) at three different peak laser intensities: $I_0 = 1 \times 10^{14}$ W/cm^2 (top panel), $2I_0$ (middle panel), and $3I_0$ (lower panel).

regularization parameter $\epsilon = 0.01$ considered in the present work.

We start out by comparing the CVA (Fig. 1, second panel from the top) results with those of the TDSE at three different laser intensities in Fig. 2. The harmonic spectra are drawn in thick red and thin black lines for the CVA and the TDSE, respectively. The generated yields based on the intensities $I_0 = 1 \times 10^{14}$ W/cm^2, $2I_0$, and $3I_0$ are shown in descending order. We see that the general shape of the harmonic spectrum and the position of the cutoff are reasonably well reproduced with the CVA approach, even though it seems to underestimate the strength of the harmonic spectra at the lowest intensity (I_0) by 2–3 orders of magnitude. The CVA results depict a cutoff at about the 23rd, 33rd, and 45th harmonics for the three laser intensities considered, which is in close agreement with the prediction of the well-known cutoff "law" $N_{\rm max} \simeq (I_p + 3U_p)/\omega_0$ [2], where I_p is the ionization potential and $U_p = A_0^2/4$ is the ponderomotive energy.

We then compare the "full" SFA results (Fig. 1, third panel from the top) with those of the TDSE for the same three laser pulses considered in Fig. 2. The harmonic spectra are shown in Fig. 3 and drawn in thick blue and thin black lines for the SFA and the TDSE, respectively. Comparing Figs. 2 and 3, it is evident that the CVA in general performs better than the SFA as far as the strength of each respective harmonic is concerned. This applies in particular to the plateau region where clear discrepancies between the TDSE and the SFA are depicted. In the cutoff region, on the other hand, the CVA and the SFA give very similar results, and both compare well with the TDSE results for the two highest laser intensities considered. Furthermore, the SFA predicts the correct position of the cutoff.

In general, the SFA seems to underestimate the harmonic yield. In particular, for the lower intensity (Fig. 3, top panel) we note that on an absolute scale the SFA shows a strong disagreement with the TDSE result around the 10th to the15th harmonics, which correspond to small electron continuum energies. At these energies it seems reasonable to assume that the Coulomb field plays an important role as illustrated by the better performance of the CVA method. For the same reason it is interesting to observe that the SFA method performs

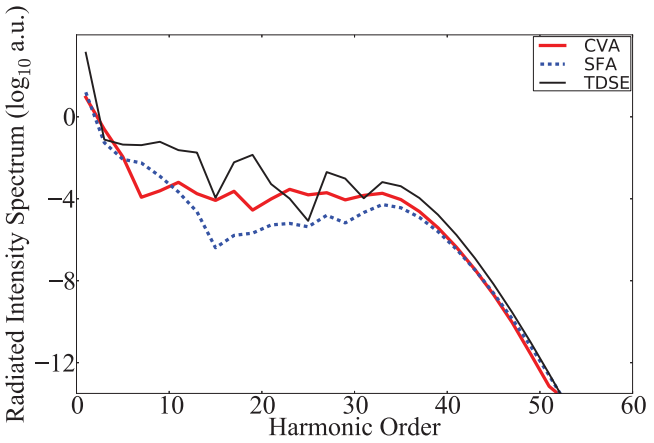

FIG. 4. (Color online) HHG spectrum [Eq. (5)] calculated based on the two approximate approaches, the SFA and the CVA, respectively, versus the exact result calculated from the TDSE. The spectra, $I_{\rm rad}(\omega)$, are shown on logarithmic scale and the peak laser intensity is $2I_0$. Thick red line: Peak harmonics from the CVA. Dotted blue line: Peak harmonics from the SFA. Thin black line: The TDSE result.

gradually better at higher laser intensities when the Coulomb potential plays a less important role.

For illustrative purposes, the harmonic spectra are shown in Fig. 4 where only the maximal values at each odd harmonic are drawn. Here, the intermediate laser intensity $I_0 = 2 \times 10^{14}$ W/cm^2 is shown as an example, but the general trends apply to the other intensities as well. Again, apart from two harmonics (numbers 7 and 25 in the spectrum), the overall picture is that the CVA performs better than the SFA as far as the strength of the harmonics is concerned, in particular in the plateau region. As such, these results show that the target distortion plays a non-negligible role in the HHG process and that approaches which include Coulomb effects are advantageous when applying approximate models.

We then turn to the stationary phase results. The upper panel in Fig. 5 shows a comparison between the exact SFA result (thin blue curve) and the result obtained based on the SPSFA amplitude [Eq. (16)], for three different values of the regularization parameter $\epsilon = 0.01$ (black curve), 0.1 (green curve), and 1 (red curve), and also for the intermediate laser intensity $I_0 = 2 \times 10^{14}$ W/cm^2. As apparent from the figure, the stationary phase results strongly depend on the choice of ϵ, in particular for the lower harmonics (up to roughly the 29th harmonic) as well as for the very highest harmonics beyond the 45th one. In the intermediate region, i.e., between the 29th and 45th harmonics, the results turn out to be less sensitive to the choice of regularization. As such, the validity of the stationary phase approximation is severely limited to harmonics in the immediate neighborhood of the cutoff. This conclusion is perhaps not unexpected, considering the fact that the integral in Eq. (16) is inherently divergent in the limit $t' \to t$, corresponding to infinitesimally short electron trajectories and an associated low-order harmonic generation.

A common way to circumvent the problem of the divergence in Eq. (16) in the limit $\epsilon \to 0$ is to apply the SPA a second time, but now to the time integral instead, set ϵ to zero, and then drop the stationary phase point at time $t' = t$. Here we propose a somewhat different approach based

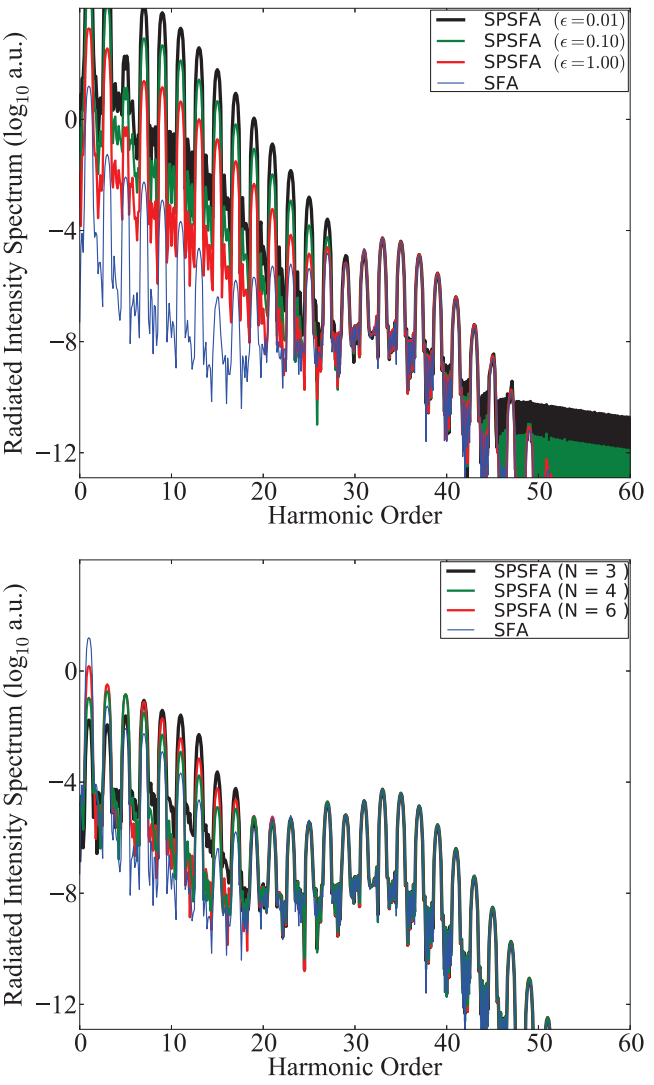

FIG. 5. (Color online) Upper panel: HHG spectrum, $I_{\rm rad}(\omega)$ [Eq. (5)], plotted on a logarithmic scale, based on fully (numerically) integrated SFA [Eq. (11)] (thin blue curve) at the peak laser intensity $2I_0$ compared with the SPSFA result [Eq. (16)] for three different values of the regularization parameter: $\epsilon = 0.01$ (black curve), 0.1 (green curve), and 1 (red curve). Lower panel: Same as upper panel, but now a comparison with the modified SPSFA result obtained by Eq. (17) for three different values of the constant N in the upper integration limit: $N = 3$ (black curve), 4 (green curve), and 6 (red curve).

on some known physical properties of the system. In the limit $t' \to t$, by definition, the electron only spends a short time in the continuum, i.e., only a fraction of a field period, before it recombines with the nucleus, and as such it does not have time to gain much kinetic energy in the field. By performing classical simulations and neglecting the effect of the Coulomb potential on the motion of the electron, just like in the SFA, one can explicitly show that trajectories corresponding to the electron being accelerated for less than a quarter of a field period before it recombines only contribute to the generation of lower-order harmonics [34]. This means that times such that $t \sim t'$ exclusively correspond to the emission of low-order-harmonic radiation and that only the lower part

of the spectrum is supposedly affected by the divergence in the integral. Based on this observation, we suggest that it might be advantageous to remove any contribution from short trajectories in the integral Eq. (16). As such, the upper limit in the integral is modified accordingly, so that only those trajectories corresponding to the electron spending more than some fraction of the laser period in the continuum before it recombines are taken into account, i.e.,

$$\langle \Psi | \, \mathbf{p} \, | \Psi \rangle = \mathrm{Re}\left\{ -i \int_{-\infty}^{t-T/N} e^{iE_i(t-t')} \, R_{\mathrm{ion}}(\mathbf{k_s}, t') \, V_{\mathrm{rec}}(\mathbf{k_s}) \right.$$
$$\left. \times \, e^{-iS(\mathbf{k_s},t,t')} \left(\frac{2\pi}{i(t-t')} \right)^{3/2} dt' \right\}, \qquad (17)$$

where T is the period of the laser field and N is some positive constant. With this modification the singularity in the SPSFA model is removed and the value of the regularization parameter ϵ can safely be set to zero. The clear advantage of this alternative choice of regularization is that the integrand now remains mathematically correct and the new regularization parameter N has a clear intuitive interpretation related to the minimum time interval between ionization and recombination.

The lower panel in Fig. 5 shows a comparison between the exact SFA result (thin blue curve) and the result obtained based on the modified SPSFA amplitude [Eq. (17)], for three different choices of the upper integration limit, corresponding to three different values of the constant N, i.e., $N = 3$ (black curve), 4 (green curve), and 6 (red curve). Comparing the upper and lower panels, it becomes clear that the spectra based on the modified SPSFA are less sensitive to the choice of regularization parameter (N) as compared to the results obtained with the standard regularization approach (ϵ) and that the modified method compares better with the exact SFA. This improvement applies to all harmonics in the spectrum. Furthermore, it is found that the harmonics beyond the 19th one are essentially unaltered by the three choices of the constant N. For the lower harmonics discrepancies are displayed, which is expected since contributions from short trajectories have been omitted. One interesting finding is that, as a rule of thumb, the harmonic signal tends to be higher when contributions from the short trajectories are left out. The effect is especially pronounced at the 15th harmonic, where the numerically integrated SFA signal is clearly suppressed with respect to the others. This means that the contributions from short and long trajectories in effect interfere destructively in the lower part of the spectrum. Inspecting the corresponding exact TDSE result (middle panel in Fig. 3) a similar suppression is seen at the 15th harmonic. As such, even the modified SPSFA method, which obviously does not display the suppression at this particular harmonic, should be used with care at the lower part of the spectrum.

Figure 6 shows a comparison of the high-harmonic spectra as obtained by the modified SPSFA amplitude in Eq. (17) and the exact (numerically integrated) SFA results, for the three intensities $I_0 = 1$, 2, and 3×10^{14} W/cm^2. Only those trajectories corresponding to the electron spending more than a quarter of a period in the continuum before it recombines are taken into account in the SPSFA amplitude, i.e., $N = 4$. As it turns out, there is now a high degree of (qualitative) agreement for all intensities and for all harmonics ranging from

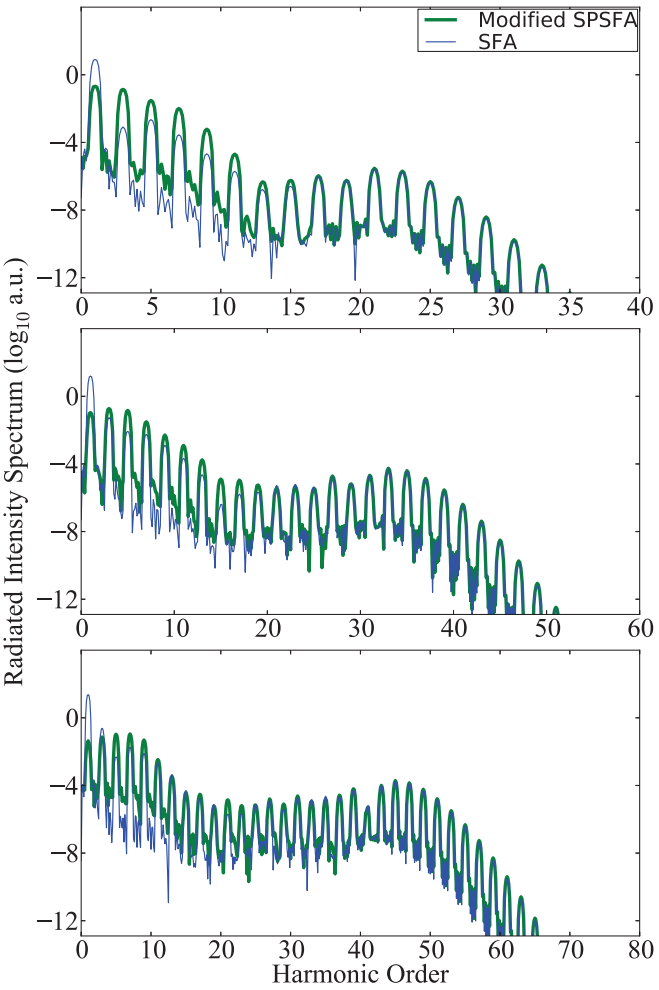

FIG. 6. (Color online) HHG spectrum, $I_{\mathrm{rad}}(\omega)$ [Eq. (5)], plotted on a logarithmic scale, from the modified SPSFA method [Eq. (17)], using $N = 4$ as the regularization, compared with exact SFA results (thin blue line) at three different peak laser intensities: $I_0 = 1 \times 10^{14}$ W/cm^2 (top panel), $2I_0$ (middle panel), and $3I_0$ (lower panel).

the lowest (except possibly the first ones as well as the above-mentioned 15th harmonic in the intermediate spectrum) to the highest. Still, a more careful inspection of the lower-lying harmonics (before the plateau region) reveals some deviation on the absolute scale. It should here be noted that the SFA (even beyond the SPA) in itself is questionable in the low-harmonic limit, as the Coulomb potential can no longer be neglected and excited bound states (that are not accounted for in the SFA) become important in the HHG process. However, as far as the higher-lying harmonics are concerned, i.e., harmonics located from the start of the plateau region and beyond, the Coulomb potential is assumed to play a less important role. The results in Fig. 6 also clearly demonstrate that short trajectories associated with the continuum electron being born and recombined during less time than a quarter-cycle are of less importance in this upper region.

IV. CONCLUDING REMARKS

In this work we have explored three sets of approximate methods to calculate the harmonic generation from hydrogen.

We have presented harmonic spectra obtained by applying the SFA, the CVA, and the SFA with the SPA applied to the momentum integrals. We expect that the obtained results are general and valid for other atomic systems as well. In general, all the approximate models studied here seem to capture the overall shape of the high-harmonic spectrum as well as giving a precise prediction of the cutoff position. However, the approximate methods seem to underestimate the harmonic yield and fail to describe detailed structures. It has also been shown that the CVA in general performs better than the SFA for intermediate and low laser intensities. Furthermore, we have demonstrated that the SPSFA performs almost at random regarding the strength of the lowest harmonics, while it is rather parameter insensitive at the end of the harmonic plateau region as well as in the cutoff. This indicates that studies of structures in the harmonic spectra must be performed with great care if the SPA is applied to the momentum integrals of the SFA. However, by removing the contribution from short electron trajectories (short times in the continuum) the resultant modified SPSFA performs rather well, almost like the fully integrated SFA.

ACKNOWLEDGMENTS

This work was supported by the Bergen Research Foundation (BFS) and the EU Seventh Framework Programme under Grant No. PIRSES-GA-2010-269243.

[1] P. B. Corkum, Phys. Rev. Lett. **71**, 1994 (1993).
[2] M. Lewenstein, Ph. Balcou, M. Yu. Ivanov, A. L'Huillier, and P. B. Corkum, Phys. Rev. A **49**, 2117 (1994).
[3] S. L. Chin and P. A. Golovinski, J. Phys. B **28**, 55 (1995).
[4] C. Lyngå, A. L'Huillier, and C.-G. Wahlström, J. Phys. B **29**, 3293 (1996).
[5] A.-T. Le, R. Della Picca, P. D. Fainstein, D. A. Telnov, M. Lein, and C. D. Lin, J. Phys. B **41**, 081002 (2008).
[6] A. Etches and L. B. Madsen, J. Phys. B **43**, 155602 (2010).
[7] S. A. Sørngard, S. I. Simonsen, and J. P. Hansen, Phys. Rev. A **87**, 053803 (2013).
[8] S. I. Simonsen, S. A. Sørngard, M. Førre, and J. P. Hansen, J. Phys. B **47**, 065401 (2014).
[9] G. Vampa, C. R. McDonald, G. Orlando, D. D. Klug, P. B. Corkum, and T. Brabec, Phys. Rev. Lett. **113**, 073901 (2014).
[10] P. Antoine, A. L'Huillier, and M. Lewenstein, Phys. Rev. Lett. **77**, 1234 (1996).
[11] A. Kamor, C. Chandre, T. Uzer, and F. Mauger, Phys. Rev. Lett. **112**, 133003 (2014).
[12] M. F. Ciappina, C. C. Chirilă, and M. Lein, Phys. Rev. A **75**, 043405 (2007).
[13] M. F. Ciappina, J. Biegert, R. Quidant, and M. Lewenstein, Phys. Rev. A **85**, 033828 (2012).
[14] S. Basile, F. Trombetta, G. Ferrante, R. Burlon, and C. Leone, Phys. Rev. A **37**, 1050(R) (1988).
[15] G. Duchateau, E. Cormier, and R. Gayet, Phys. Rev. A **66**, 023412 (2002).
[16] R. Gayet, J. Phys. B **38**, 3905 (2005).
[17] R. Guichard, H. Bachau, E. Cormier, R. Gayet, and V. D. Rodriguez, Phys. Scr. **76**, 397 (2007).
[18] R. Della Picca, J. Fiol, and P. D. Fainstein, J. Phys. B **46**, 175603 (2013).
[19] D. G. Arbó, J. E. Miraglia, M. S. Gravielle, K. Schiessl, E. Persson, and J. Burgdörfer, Phys. Rev. A **77**, 013401 (2008).
[20] V. D. Rodríguez, E. Cormier, and R. Gayet, Phys. Rev. A **69**, 053402 (2004).
[21] M. S. Gravielle, D. G. Arbó, J. E. Miraglia, and M. F. Ciappina, J. Phys. B **45**, 015601 (2012).
[22] M. Yu. Ivanov, T. Brabec, and N. Burnett, Phys. Rev. A **54**, 742 (1996).
[23] J. A. Pérez-Hernández and L. Plaja, Phys. Rev. A **76**, 023829 (2007).
[24] J. A. Pérez-Hernández, L. Roso, and L. Plaja, Opt. Express **17**, 9891 (2009).
[25] L. Plaja and J. A. Pérez-Hernández, Opt. Express **15**, 3629 (2007).
[26] A. Rupenyan, P. M. Kraus, J. Schneider, and H. J. Worner, Phys. Rev. A **87**, 031401(R) (2013).
[27] X.-B. Bian, Phys. Rev. A **90**, 033403 (2014).
[28] M. Førre and A. S. Simonsen, Phys. Rev. A **90**, 053411 (2014).
[29] J. C. Baggesen and L. B. Madsen, J. Phys. B **44**, 115601 (2011).
[30] C. C. Chirilă and M. Lein, Phys. Rev. A **73**, 023410 (2006).
[31] J. Chen and S. G. Chen, Phys. Rev. A **75**, 041402(R) (2007).
[32] I. S. Reljin, B. D. Reljin, and V. D. Papić, IEEE Trans. Instrum. Meas. **56**, 1025 (2007).
[33] S. Datta, J. Phys. B **18**, 853 (1985).
[34] M. F. Ciappina, J. A. Pérez-Hernández, and M. Lewenstein, Comput. Phys. Commun. **185**, 398 (2014).